Combustion and Flame 160 (2013) 2770–2782

Contents lists available at SciVerse ScienceDirect

Combustion and Flame

journal homepage: www.elsevier.com/locate/combustflame

Structure of laminar premixed flames of methane near the auto-ignition limit

Peter Habisreuther *, Flavio Cesar Cunha Galeazzo, Chockalingam Prathap, Nikolaos Zarzalis

Engler-Bunte-Institute, Division of Combustion Technology, Karlsruhe Institute of Technology, Karlsruhe, Germany

ARTICLE INFO

Article history:
Received 9 November 2012
Received in revised form 20 March 2013
Accepted 20 June 2013
Available online 19 July 2013

Keywords:
High temperature combustion
Freely propagating planar flames
Auto-ignition
Ignition delay time
Laminar burning velocity
Pressure dependency

ABSTRACT

Auto-ignition and flame propagation are the two different controlling mechanisms for stabilizing the flame in secondary stage combustion in hot vitiated air environment and at elevated pressure. The present work aims at the investigation of the flame stabilization mechanism of flames developing in such an environment. In order to better understand the structure of turbulent flames at inlet temperature well above the auto-ignition temperature, the behavior of laminar flames at those conditions needs to be analyzed. As an alternative to challenging and expensive measurements at high temperature and pressure, the behavior of laminar flames at such conditions can be predicted from theory using mathematical simulation. In the present work, the laminar burning velocities and flame structures of premixed stoichiometric methane/air mixtures for inlet temperatures from 300 to 1450 K and absolute pressures from 1 to 8 bar have been calculated using a freely propagating laminar, one dimensional, planar flame model. The prediction shows that at inlet temperatures below the auto-ignition temperature, the predicted laminar burning velocity which corresponds to the unburned mixture velocity in order to create a steady laminar flame decreases with increase in pressure. When the inlet temperature of the mixture goes well beyond the auto-ignition temperature of the mixture, however, the unburned mixture velocity increases steeply at higher pressure level, because of a complete transition of the flame structure.

1. Introduction

Interest in new combustion concepts has grown significantly in the last few decades, mainly driven by the need of environmentally friendly processes. One of the leading concepts is High Temperature Air Combustion (HiTAC) in which the air is preheated using preheating by regenerative systems above the self ignition temperature of the mixture. With this concept dilution of the oxidizer with recirculated exhaust gases inside the combustor prior to combustion results in low levels of oxygen concentration which subsequently generates low nitric oxide emissions. The advantages of HiTAC are, therefore, low pollutant emission levels and high energy efficiency. This concept is called also Flameless Oxidation or Mild Combustion [1–3]. Another successful technology is the Reheat Gas Turbine Technology or Sequential Gas Turbine Technology where the excess enthalpy and the remaining oxygen in the exhaust gases after the primary turbine stage are used to combust fuel or fuel–air mixture by injecting them into the exhaust gases [4]. The exhaust gases have high temperature, i.e., above the auto-ignition temperature of the mixture injected, and low oxygen concentration. This concept results in high efficiency, good operational flexibility and low pollutant emission. Hayashi and Yamada [5] reported that under these conditions, flame stabilization in the exhaust gases is due to auto-ignition. They developed a two-stage combustion system in which the first stage operates in a lean premixed mode, and in the secondary stage, a lean premixed fuel–air mixture is injected into the exhaust gases of the primary stage. The temperature of the exhaust gases from the primary stage is significantly higher than the auto-ignition temperature of the secondary stage mixture, resulting in stabilizing the secondary stage combustion. They reported several advantages of this staged combustion system, like very low NO_X emissions and wider operational limits compared to a single staged combustion system. Later, they tested this system for higher pressures and also extended it to a three-stage combustion system for the utilization of low calorific fuels. They did not comment on the stabilization mechanism of the flames anchored in the second stage. Similarly, in a recent work Prathap et al. [6] performed emission measurements in a two-stage combustion system where the primary stage operated in a lean mode to generate vitiated air with the following characteristics: $T = 1473–1673$ K, mole fraction of O_2 in the vitiated air = 8–10% and $p_0 = 5–8$ bar. In the secondary stage, methane was injected at an angle of 30° into the cross flow of vitiated air. They measured the penetration depth of the secondary stage flame using a

* Corresponding author. Address: Engler-Bunte-Ring 1, D 76131 Karlsruhe, Germany. Fax: +49 721 608 47770.
E-mail address: Peter.Habisreuther@kit.edu (P. Habisreuther).

0010-2180/$ - see front matter © 2013 The Combustion Institute. Published by Elsevier Inc. All rights reserved.
http://dx.doi.org/10.1016/j.combustflame.2013.06.023

Nomenclature

α^*	effective thermal diffusivity (m^2/s)
c_p	mixture averaged heat capacity at constant pressure (J/kg K)
h	specific enthalpy (J/kg)
p	pressure (Pa)
q	net rate of progress of a reaction (mol/m^3 s)
u	velocity of fluid mixture (m/s)
t	time (s)
A	cross sectional area (m^2)
$\dot{M}$	mass flow rate (kg/s)
N_R N_S	number of considered reactions or species in a chemical kinetic scheme
$\overline{R}$	universal gas constant (J/mol K)
S_L	laminar burning velocity (m/s)
T	temperature (K)
V_k	diffusion velocity of the kth species (m/s)
W	molar mass (kg/mol)
Y	mass fraction
x	1D spatial coordinate (m)

Greek

λ	thermal conductivity (W/m K)
v	stoichiometric coefficient of a species in a reaction
ρ	mass density (kg/m^3)
$\dot{\omega}$	molar rate of production (mol/m^3 s)
τ_{HR}	characteristic time scale of heat release (s)
ξ	time integral contribution of a reaction to the formation of a species
ϕ	equivalence ratio
τ_{id}	ignition delay time

Subscripts

0	unburned gas
b	burned gas
k	kth species
i	ith reaction
L	laminar
tp	point of inflection

movable gas suction probe and reported that penetration depth measured at 8 bar is less than compared to the penetration depth measured at 5 bar. They mentioned that the flame at 8 bar, under the operating conditions studied, was more reactive than the flame generated at 5 bar, and they supported this result by numerical simulation. The possible flame stabilization mechanism in the secondary stage could be either auto-ignition or turbulent flame propagation. In contrary to results reported by Prathap et al. [6], the laminar burning velocity of methane–air flames at ambient temperature decreases with an increase in pressure [7,18–20]. No literature data on burning velocity are available for the operating conditions realized by Prathap et al. [6].

A widely used property for the characterization of reactivity of combustible mixtures together with molecular transport is given by the propagation speed of the laminar, premixed, 1-d flame. Together with turbulence parameter this property exhibits a basis for the numerical description as well as for the design of real combustion devices. Unfortunately, at the ultra-high preheating temperatures of more than 1000 K experiments on laminar, premixed flame propagation can hardly be performed and therefore numerical simulations using detailed reaction schemes are often used. In the present work, numerical simulations of methane–air flames have been conducted at pressures ranging from 1 bar to 8 bar and for initial temperatures ranging from 300 K to 1450 K, in order to further investigate the reason for the change in reactivity with the change of pressure as reported by Prathap et al. [6]. At high temperatures it was found that the laminar flame speed exhibits extremely high values that can hardly be explained by the balance of heat release and molecular heat transport alone. Therefore, it was suspected that auto-ignition plays a major role for the stabilization of flames under these conditions and the basic intention of the current work was to get knowledge on the flame behavior when auto-ignition overtakes flame propagation as stabilizing mechanism.

Zabetakis [9] had reported that the auto-ignition temperature of methane at atmospheric pressure is 810 K. Smyth and Bryner [10] reported that auto-ignition temperature of a combustible mixture strongly depends on the residence time of the combustible mixture at or near to the heat source on the equivalence ratio, and the temperature of the heat source. They found that the auto-ignition temperature of stoichiometric methane–air mixtures at 1 bar and for a residence time of less than 130 ms is 1087 ± 10 K, measured in the presence of stainless steel foil, and 1313 ± 10 K, measured with nickel foil. Caron et al. [11] measured the auto-ignition temperatures of methane–air mixtures for ϕ = 4.08–46.48 at 2–47 bar and indicated that auto-ignition temperature is a strong function of pressure and decreases with increase in pressure. Although they did not measure the auto-ignition temperature for stoichiometric methane–air mixture, it becomes evident from their study that the same behavior would apply for stoichiometric methane–air mixtures. Many of the early experimental results of methane/oxygen ignition delay [12–16] were correlated with initial conditions using an Arrhenius-type formula and the concentrations of oxygen and methane which indicates that the type of dilution gas has negligible effect on the delay time. Huang et al. [17] summarized these correlations and compared them to own measurements.

2. Computational methods

In the present study, the numerical simulations of steady-state, one-dimensional laminar premixed flames were performed using the code PREMIX [22]. The PREMIX code solves the one-dimensional, laminar, steady state equations of continuity, species and energy balance. It accounts for finite-rate chemical kinetics and multi-component molecular transport. The freely propagating planar flame model was used along with the mixture averaged transport properties evaluated using the CHEMKIN-II subroutine library [23]. This model imposes that the mass flux $\dot{M}$ is an eigenvalue of the problem and must be determined as a part of the solution. The additional condition that is required in this context in order to reduce the problem by one degree of freedom is chosen by fixing the location of the flame through specifying the temperature at one point. For this condition an additional requirement is that the domain has to be sufficiently large to ensure that all gradients at the inlet and outlet boundary vanish. At the inlet or cold flow boundary the mass flux fractions and the temperature is specified, while at the outlet or hot boundary all gradients are specified to vanish. The solution is calculated on an adaptive mesh that takes into

account a relative gradient and curvature of the solution vector. In order to ensure an accurate converged and grid independent solution, the adaptive mesh criteria for the largest relative gradient and curvature were toughly selected as 0.04 and 0.07. The equations governing steady, isobaric, quasi-one-dimensional flame propagation used by PREMIX are as follows [22]:

$$\text{Continuity} \quad \dot{M} = \rho u A \tag{1}$$

$$\text{Energy} \quad \dot{M}\frac{dT}{dx} - \frac{1}{cp}\frac{d}{dx} + \left(\lambda A \frac{dT}{dx}\right) + \frac{A}{cp}\sum_{k=1}^{K}\rho Y_k V_k c_{pk}\frac{dT}{dx} + \frac{A}{cp}\sum_{k=1}^{N_s}\dot{\omega}_k h_k W_k = 0 \tag{2}$$

$$\text{Species} \quad \dot{M}\frac{dY_k}{dx} + \frac{\partial}{\partial x}(\rho A Y_k V_k) - A\dot{\omega}_k W_k = 0 \quad (k = 1, \ldots, K) \tag{3}$$

$$\text{Equation of State} \quad \rho = \frac{p\overline{W}}{RT} \tag{4}$$

The individual contribution of the different terms of the energy equation for a given set of operating condition is required in this work for the discussion of the results. The four terms of the energy equation, as to be observed from left to right, are: (1) heat convection, (2) heat conduction, (3) thermal diffusion and (4) heat release due to chemical reaction.

The following chemical-kinetic reaction mechanisms were used: the GRI 3.0 [24], GRI 2.11 [25], UBC 2.1 [30], LEEDS [26] and SAN DIEGO (USCD) [27] mechanisms for methane, and the *n*-decane mechanisms developed by Honneta et al. [28] (referred to as RWTH) and developed by Muharam and Warnatz [29] (referred to as IWR). As the present simulations involve high pressure and temperature of premixed methane/air mixtures, it is important to validate the chemical kinetic schemes used in the present work with the experimental data available in the literature. Ogami and Kobayashi [7] had measured the laminar burning velocity, S_L, of CH_4–air and CH_4–air–He mixtures using the burner method at elevated pressures and temperatures. To predict the laminar burning velocities of CH_4–air–He mixtures measured by Ogami and Kobayashi [7], the Chaperon efficiencies of helium are needed. In the present work, the Chaperon efficiencies of argon have been used for helium due to their thermo-chemical similarity as proposed by Kwon et al. [33].

In the present work, simulations have been conducted for stoichiometric methane–air-helium mixtures, varying for validation purposes inlet temperatures from 400 to 600 K and pressures from 1 to 7 bar with the GRI 3.0 chemical mechanism. After that, laminar burning velocities of stoichiometric methane–air mixtures were predicted using the five detailed reaction mechanisms GRI 3.0, GRI 2.11, UBC 2.1, IWR and RWTH for initial temperatures varied from 298 to 1450 K and for pressures varied from 1 to 8 bar. Despite the fact that the RWTH and IWR chemical-kinetic schemes have been optimized for isomers of decane, their application to methane is feasible because of their hierarchical structure. Laminar burning velocity, i.e. the velocity of the incoming mixture normal to the flame front, has been predicted for the above mentioned operating conditions and is being discussed in the following sections.

3. Results and discussion

3.1. Validation

It is essential to validate the present numerical procedure and the implemented different kinetic schemes with measured data from literature. Hence, simulations have been conducted for all the operating conditions of the measured burning velocity data of Ogami and Kobayashi [7]. Figure 1 shows the comparison of the predicted laminar burning velocity of stoichiometric methane–air mixtures diluted with 10% helium by volume with the Ogami and Kobayashi [7] measured and calculated data for unburned mixture temperatures of 400 and 600 K and at varying initial pressures ranging from 1 to 8 bar. The GRI 3.0 reaction mechanism was used in our PREMIX simulations as well as in [7]. The agreement of the simulations with the measurements is very good and even outreaches the agreement that was obtained by Ogami and Kobayashi using the same chemical scheme. This can be attributed to the very fine resolution in the current simulations that was forced by the very strict convergence criteria used, as mentioned above. At 600 K, the present simulation slightly under predicts the laminar burning velocity at 5 and 7 bar, but the error remains low. Figure 1 shows that both, the predicted and measured burning velocities decreased with an increase in initial pressure for both the initial temperatures 400 and 600 K.

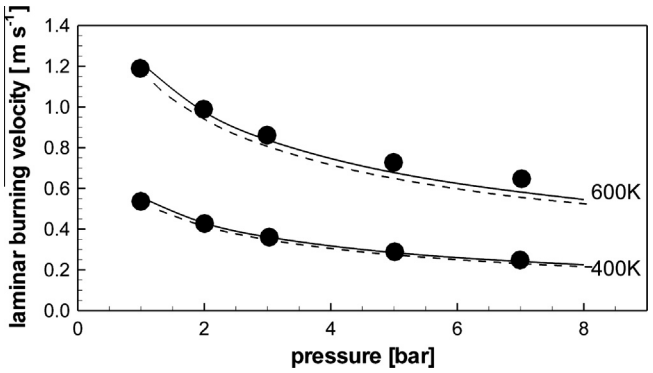

Fig. 1. Variation of laminar burning velocity S_L with pressure for CH_4/air/He mixture, $\phi = 1.0$, He = 10% in volume. Solid lines, present simulations; symbols denote measurements and dashed lines simulations from Ogami and Kobayashi [7].

3.2. Effect of initial temperature of reactants on burning velocity

As explained in the preceding sections, in new combustion concepts, the initial temperature of the reactants is chosen well above the auto-ignition temperature of the reactants. Hence, in the present work the laminar flame characteristics of stoichiometric methane–air mixture for initial temperature values ranging from 300 to 1450 K at 1 bar are studied. The predicted laminar burning velocities of stoichiometric methane–air mixture for 600 K and 1450 K, i.e., typical temperatures in the experiments of Prathap et al. [6], at 1 bar are shown in Fig. 2. Initially, the GRI 3.0 chemical-kinetic scheme was used. At 600 K, the laminar burning velocity scales down with increasing pressures, and this trend of burning velocity decreasing with pressure had been frequently reported in the literature [7,18–20]. However, at an initial temperature of 1450 K and when keeping all other operating conditions constant, Figure 2 shows very high values of burning velocity compared to 600 K, and moreover the burning velocity increases with increasing initial pressure. In order to assure that this result is not a spurious effect of the chemical-kinetic scheme, different chemical mechanisms have been implemented in the present simulations for cross-validation and the results are also shown in Fig. 2. It is necessary to specify that none of the implemented reaction mechanisms had been validated at 1450 K. Although the scatter in the magnitude of the predicted values of burning velocity with different chemical schemes is evident, the trend of variation for the burning velocity with increasing pressure is the same for all reaction mechanisms. As the calculated burning velocity of the stoichiometric methane/air mixture at 1 bar and 1450 K is substantially higher than the values at 600 K it is not clear whether the denotation

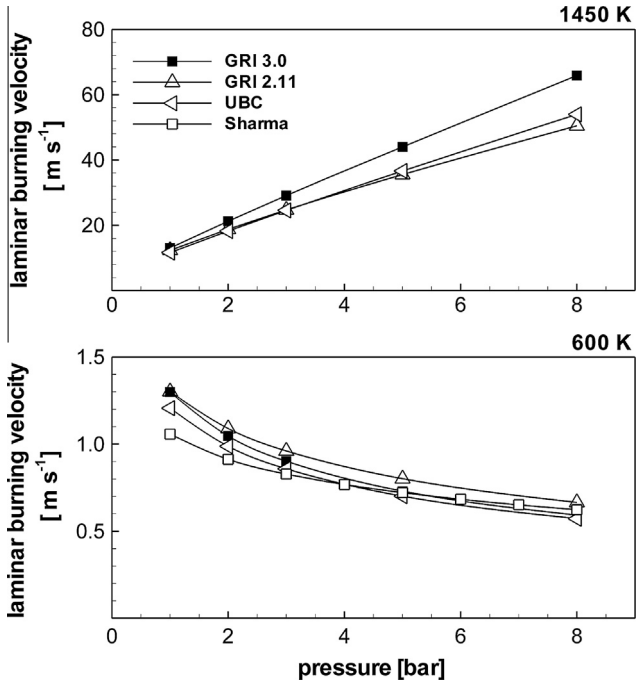

Fig. 2. Laminar burning velocity S_L over pressure of stoichiometric methane/air mixture using different reaction mechanisms. Unburned mixture temperature is 1450 K (top) and 600 K (bottom).

"burning velocity" is justified in all cases reported. Therefore, in the present work it will be referred to as "velocity of incoming mixture", which is valid for any type of flame stabilization mechanism. Hence, at 1450 K, the velocity of the incoming mixture increases with an increase in the pressure and also exhibits extremely high velocities (please note the different scales of the diagrams in Fig. 2). The possible reasons and mechanisms are analyzed and discussed in the following sections.

The essential observations of Fig. 2 are: (1) the predicted laminar burning velocities of stoichiometric methane–air mixture at 600 K, which is less than auto-ignition temperature compares well with Sharma et al. [8] data; and (2) the predicted velocity of the incoming mixture at 1450 K preheating temperature, which is well above the auto-ignition temperature, from all the implemented chemical reaction schemes are extremely high. One possible reason for this increase of the velocities at the high initial temperature could be due to a corresponding increase in the magnitude of transport properties and the specific heat capacities of the reactants. But this reason is not sufficient to explain the order of magnitude increase in the burning velocities between 600 and 1450 K. The second possible explanation could be that the chemical reaction follows a different path for very high initial temperatures, resulting in high reaction rates and higher velocities. Hu et al. [21] investigated the influence of chemical kinetics on the flame speed of methane–hydrogen–air flames at moderately elevated temperatures (up to 450 K) and stated that the laminar burning velocity is depended on the competition between the main chain branching reactions and chain recombination reactions. They concluded that with an increase of initial temperature, the two-body chain branching reactions are temperature-sensitive, and the recombination reactions represent temperature-insensitive three-body reactions. The branching reaction and recombination reaction are enhanced relative to each other by increasing the flame temperature and system pressure, respectively. Nevertheless, the overall sensitivity decreases when increasing the preheating temperature.

In order to understand the change in the reaction rate of the different reactions in the GRI 3.0 reaction mechanism with a massive increase of initial temperature in the current work a reaction flux analysis on basis of the species profiles of laminar flame calculations using the GRI 3.0 mechanism for two different preheating temperatures such as 298 K and 1450 K at 5 bar has been undertaken. It has to be mentioned that the analyzed profiles, being a result of the laminar flame calculations, represent the result of reactive conversion as well as diffusive transport. For stoichiometric methane–air mixture at 5 bar the corresponding predicted laminar burning velocities or velocities of incoming mixture are 0.73 m/s for 600 K and 35.53 m/s for 1450 K initial temperature, which represents an increase of almost two orders of magnitude. Figure 3 shows the time integral contributions of all reactions of the GRI 3.0 chemical-kinetic scheme that contribute to the methane conversion, normalized by the time integral value of the net conversion rate of methane:

$$\xi_{CH_4 i} = \frac{\int_0^\tau \nu CH_{4,i} \cdot q_i \, dt}{\int_0^\tau \left(\sum_{j=0}^{N_R} \nu_{CH_4 j} \cdot q_j \right) dt} \tag{5}$$

with $\nu_{CH_4 i}$ denoting the stoichiometric coefficient of methane in reaction i, q_i the net rate of progress of reaction i and N_R being the number of reactions.

Figure 3 shows that at 600 K, the intermediate reactions involving methane with OH, H and O are predominant, and a significant contribution stems also from the third-body break-up of methane. At an initial temperature of 1450 K, the relative contribution of the break-up reaction 52 is reduced, and subsequently the contribution of the reaction with HCO (reaction 161) is increased.

Although these small differences are also not appropriate to explain the increase of the incoming mixture speed at 1450 K compared to that of 600 K by two orders of magnitude, they give a hint on the underlying phenomenon: the change of the internal flame structure in terms of heat and mass transport has to be considered.

3.3. Flame structure

As the foregoing discussion could not explain the reason for the extremely high velocities at an initial temperature of 1450 K, a comparison of the flame structures is carried out in this section.

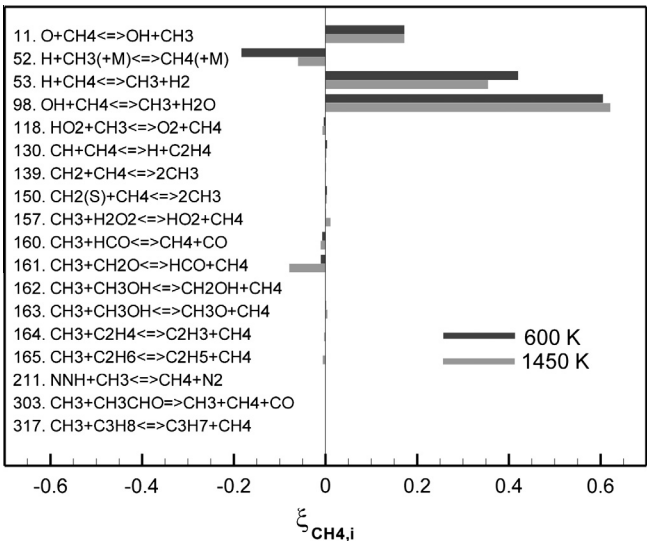

Fig. 3. Reaction flux analysis of integral contributions of selected reactions, normalized by the integral methane reaction rate for CH_4/air mixture, $\phi = 1.0$, $p_0 = 5$ bar, with unburned mixture temperatures of 600 and 1450 K using the GRI 3.0 mechanism.

Following the thermal theory of laminar flame propagation developed by Zeldovich and Frank-Kamenetsky [31] and discussed by Evans [32] the laminar flame structure is divided into a preheat and a reaction zone. In the relatively thick preheat zone, diffusive and convective transport processes dominate without any chemical reaction. In the comparatively thin reaction zone, the chemical reaction of the preheated reactants occurs, leading to intense release of thermal energy and resulting in the formation of hot products. In the reaction zone, the mass transport term is considered small compared to the other three terms in the energy equation (see Fig. 4). This theory defines the laminar burning velocity S_L as a function of an effective thermal diffusivity α^* and a characteristic reaction time, τ_{HR}:

$$S_L \propto \left(\frac{\alpha^*}{\tau_{HR}}\right)^{\frac{1}{2}}, \quad \text{with } a^* = \frac{\lambda_b}{\rho_0 c_{p,0}} \tag{6}$$

In the flame front, conduction and convection of heat from the reaction zone into the preheat zone determines the thickness of the flame and the laminar burning velocity. In order to understand the balance between heat release and transport mechanisms in the flame front, the variation of the magnitudes of the different terms in the energy equation within the flame structure of stoichiometric methane–air mixture at $T_0 = 298$ K and $p_0 = 5$ bar is plotted in Fig. 4. The dashed line represents the energy transfer due to convection from the reaction zone to the unburned reactants in the preheat zone (first term in Eq. (2)), the dash-dot-line represents the energy release due to chemical reaction (fourth term in Eq. (2)), and the continuous line represents the energy transfer due to diffusion from reaction zone to the unburned reactants in the preheat zone (summation of second and third term in Eq. (2)). It is important to mention that all the terms have been divided by the product of density and cross-sectional area to improve the readability of the profiles. In Fig. 4, the flow direction is from the left side (fresh mixture) to the right (hot products) side. Figure 4 clearly indicates that in the reaction zone the heat release term and the diffusive term balance each other, and in the preheating zone the convection and diffusive term almost balance each other.

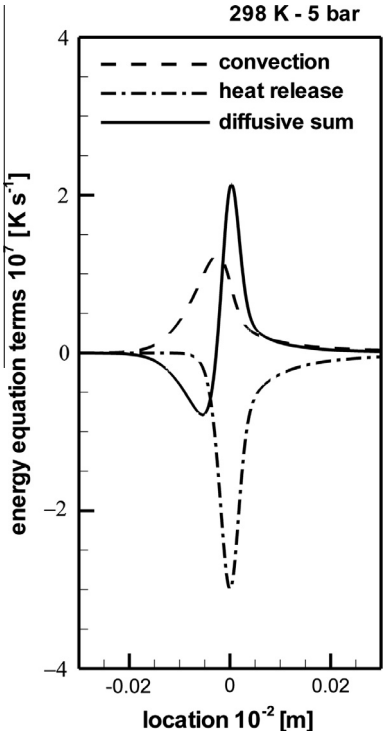

Fig. 4. Profiles of the terms of the energy equation for CH_4/air mixture, $\phi = 1.0$, $p_0 = 5$ bar and $T_0 = 298$ K.

On this basis, the variation of the different energy terms in Eq. (2) with increase in initial temperature was studied for 400 K, 600 K and 1450 K at a pressure of 5 bar for stoichiometric methane–air mixture, and the results are shown in Fig. 5. At initial temperatures, 400 K and 600 K, the profiles of the different energy terms are similar to the profiles predicted at 298 K. However, at an inlet temperature of 1450 K, which is significantly above the auto-ignition temperature of the mixture, the profiles of the different energy terms completely change when being compared to temperatures below 600 K. At 1450 K, the sum of the diffusive terms did not balance the heat release term which is substantially larger than the diffusive term. An important observation from the profiles of energy terms at 1450 K is that the chemical reaction starts in the preheat zone itself and, hence, the basic assumption of a chemically inert preheating zone becomes invalid for the preheating temperature at 1450 K. Also, the reaction zone of the flame at 1450 K is thicker than the flames studied at preheating temperatures between 298 K and 600 K. In order to have more insight into change of the flame structure for preheating temperature well above the auto-ignition temperature of the combustible mixture, the abscissa of Fig. 5 in length scale had been transformed into time scales. For that transformation from length to time the following transformation rule $dt = \rho A/\dot{M}\,dx$ has been applied. The profiles of the different energy terms at time coordinates are displayed in the bottom row of Fig. 5. For better comparability, the time coordinate in Fig. 5 has been offset by the time the reactants pass from inlet to the position of the peak value of the reaction source term. These profiles clearly demonstrate that the chemical reaction time, i.e. the duration of the heat release, is very short at 1450 K compared to the case with lower preheating temperatures, and it indicates that reaction propagates much faster at 1450 K than at the lower preheating temperatures. Also, the profiles of the energy terms at 1450 K displayed that the energy transported due to diffusion terms lose their importance as compared to the heat release and convection term. At 1450 K, the profile of the convection term almost mirrors the profile of the heat release term, while for lower preheating temperatures such at 298 K, 400 K and 600 K, energy transportation due to diffusion plays a predominant role in comparison to the convection and heat release terms. Figure 5 suggests that with increase in the preheating temperature well above the auto-ignition temperature, the importance of diffusion decreases and the structure of the flame approaches that of a plug flow reactor model in which the transport due to diffusion is being neglected completely. These observations are supported by comparing the mole fraction profiles of CH_4, CH_2O, HCO and CO for the initial temperatures 600 K and 1450 K in Fig. 6. While for the 600 K case the mole fractions remain constant up to below 1 mm prior to the flame region, in the 1450 K case the species CH_2O and HCO that are known to be important for auto ignition start to increase immediately after the inlet boundary. This also reflects the results of the reaction flux analysis shown above. For sake of a better visibility of the main reaction zone the abscissa of the right plot in Fig. 6 has been scaled towards the inlet and outlet boundary.

Similar results were obtained in calculations when using incoming mixtures that were diluted by exhaust gas when comparing the results of calculations with incoming mixtures of comparable oxygen content. This indicates that the type of dilution gas (excess air or products) has small effect on the phenomenon.

3.4. Velocity of incoming mixture or laminar burning velocity

In order to further quantify the effect of initial temperatures, either above or below the limit of auto-ignition, the velocities of

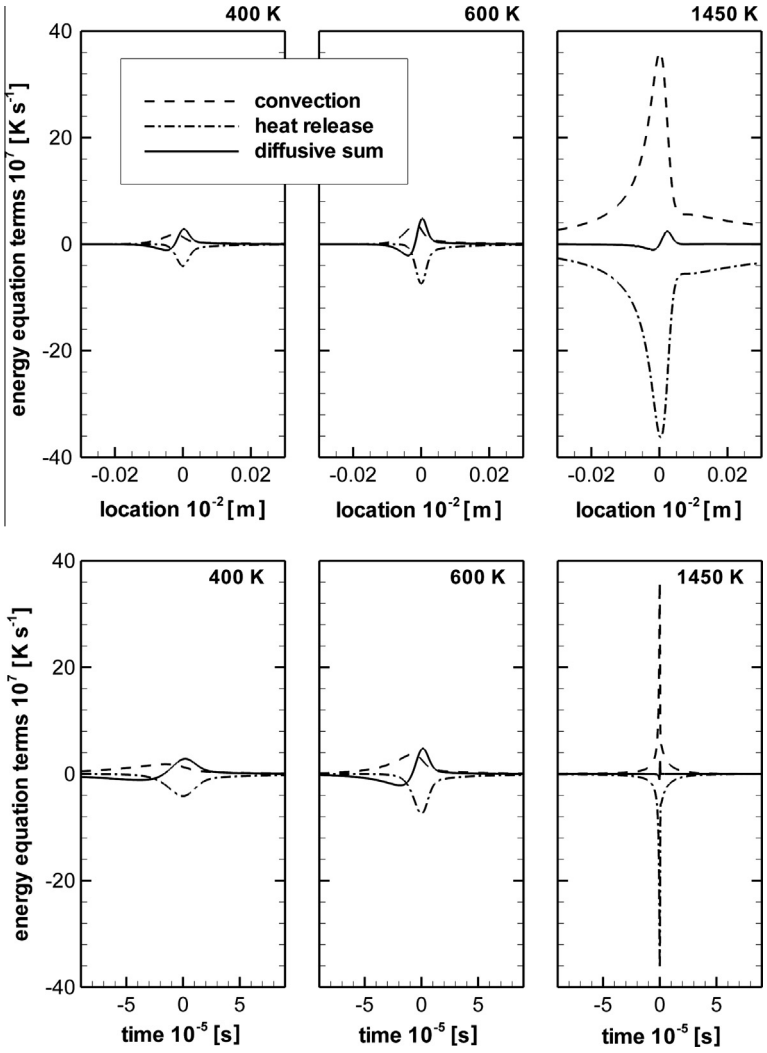

Fig. 5. Profiles of the terms of the energy equation for stoichiometric CH_4/air mixture at $p_0 = 5$ bar, and initial temperatures 400, 600 and 1450 K calculated by the GRI 3.0 mechanism. Diagrams displayed in space (top) and time (bottom) coordinates.

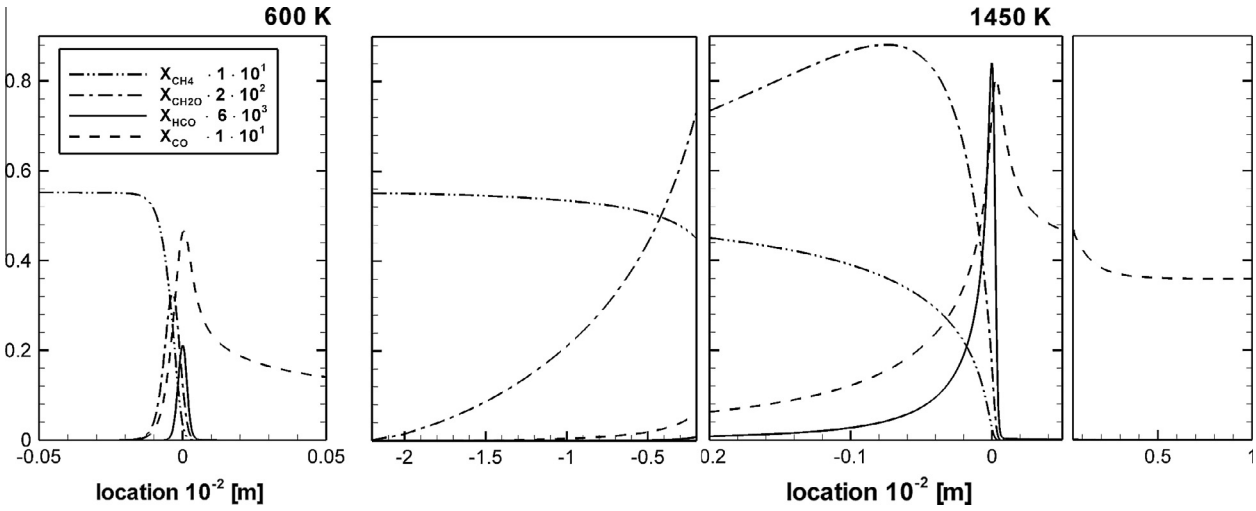

Fig. 6. Comparison of mole fraction profiles of CH_4, CH_2O, HCO and CO for laminar flame calculations of stoichiometric CH_4/air mixture at 5 bar at initial temperatures 600 K and 1450 K.

the incoming mixtures were calculated using the GRI 3.0 mechanism for stoichiometric methane/air mixture at 1 and 5 bar for different preheating temperatures and different sizes of computational domain varied from 0.32 to 1.58 m. The intention of varying the length of the computational domain was to take a look at the flame structure when the residence time of the

reactants before reaction in the calculation domain increases up to the point when auto ignition overtakes flame propagations. An additional spin-off from varying the calculation domain is that the independence of the laminar flame speed on the inlet condition could be validated. It also has to be emphasized that even after auto ignition controls the flame, the governing equations that contain diffusion and conduction terms and describe the laminar premixed 1-d flame converge for an individual, distinct inlet velocity and the used calculation domain. The resulting velocities of the incoming mixture are displayed in Fig. 7, which shows that for initial temperatures up to a certain limit, the velocity of the incoming mixture is independent of the domain size and therefore also independent on the residence time upstream of the flame and can, therefore, be called "laminar burning velocity". It is an essential result, that even for the considered large calculation domain (>1 m), this laminar burning velocity up to a specific initial mixture temperature is independent of the domain size, for preheating temperatures below 1100 K at 1 bar and 1000 K at 5 bar. These limiting temperatures are in the order of the ignition temperature of methane reported in the literature [10].

For preheating temperatures higher than the above specified limits, however, the calculated incoming mixture velocity increases much faster and also turned out to be dependent of the domain size. At these conditions the incoming mixture velocity can, therefore, no longer be termed as laminar burning velocity.

In order to acquire more information on the transition of the flame structure occurring when the initial temperature exceeds the auto-ignition temperature of the mixtures, the profiles of different terms of the energy equation of the stoichiometric methane/air mixture at 1 bar and different preheating temperatures such as 1083, 1113 and 1143 K are shown in Fig. 8. These three preheating temperatures have been chosen near to 1100 K, i.e. near the presumed transition temperature of the flame structure. The domain size used for these simulations is $\Delta x = 158$ cm (denoted by gray diamonds in Fig. 7, left). At an initial temperature of 1083 K, i.e. slightly below the steep velocity gradient in Fig. 7 the profiles of the energy terms in Fig. 8 represent laminar flame behavior, since the location of peak of the diffusion term slightly precedes the peak of the heat release term according to the thermal theory. However, at $T_0 = 1143$ K, i.e. slightly above the

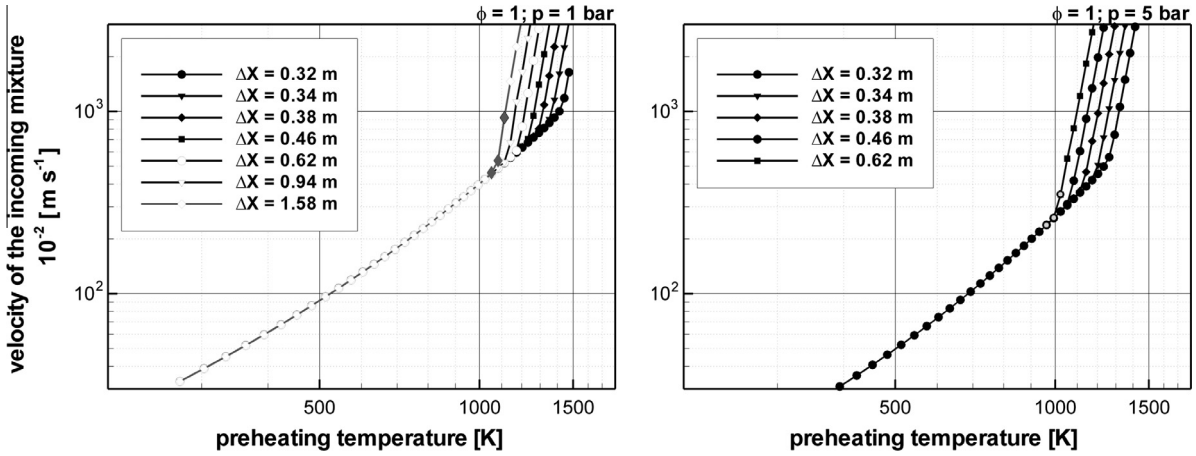

Fig. 7. Predicted velocity of the incoming mixture, i.e., laminar burning velocity, of stoichiometric CH_4/air mixture as a function of initial temperature from GRI 3.0 mechanism for different calculation domains at 1 bar (left) and 5 bar (right).

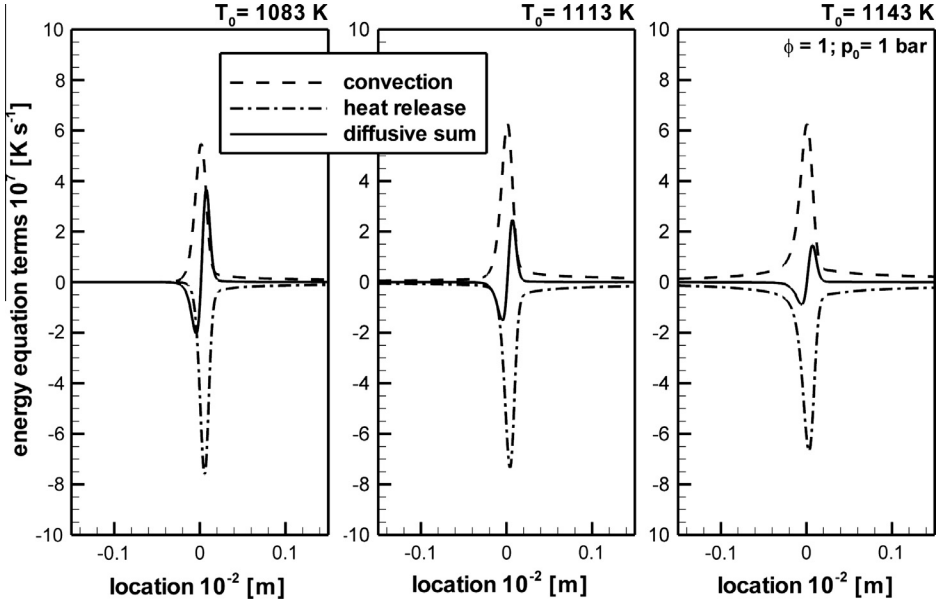

Fig. 8. Profiles of the terms of the energy equation for CH_4/air mixture, $\phi = 1.0$, $p_0 = 1$ bar, with unburned mixture temperatures T_0 of 1083, 1113 and 1143 K using the GRI 3.0 mechanism.

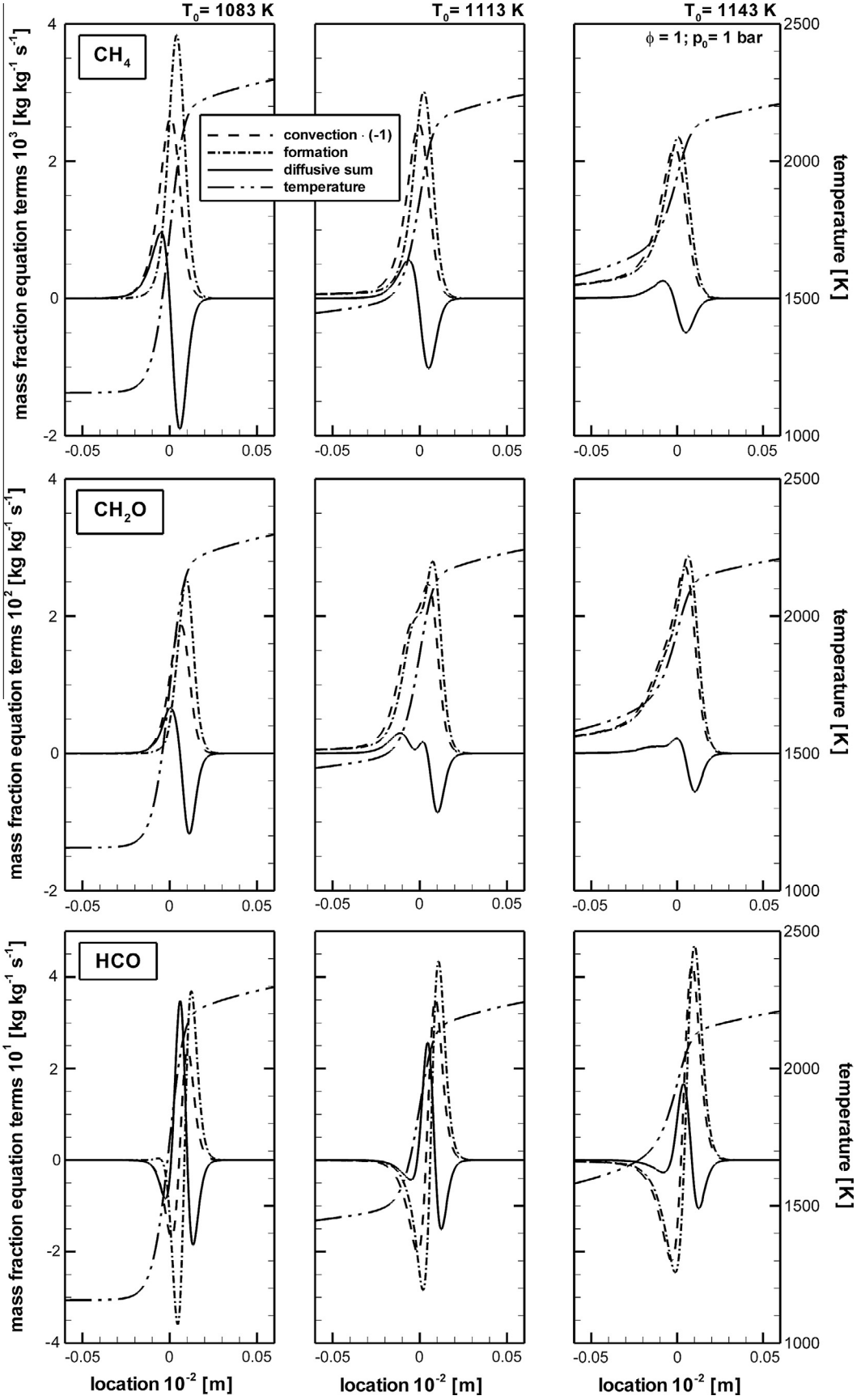

Fig. 9. Profiles of the terms of selected species mass fraction balance equations and temperature profiles at $\phi = 1.0$, $p_0 = 1$ bar, with unburned mixture temperatures T_0 of 1083, 1113 and 1143 K using the GRI 3.0 mechanism.

transition temperature Fig. 8 shows that an increase of the absolute value of the heat release term can be observed already upstream of the corresponding increase of the diffusive sum term. This correspondence indicates obviously that auto-ignition has already taken place prior to the main reaction zone, defined by the peak in the heat release term. For the intermediate case at T_0 = 1113 K, the start of increase of both, the absolute values of heat release term and the diffusive sum term spatially coincide.

A similar behavior as found for the energy balance equation can be observed when the terms of the species balance equations (Eq. (2)) are evaluated. Figure 9 depicts the profiles of the equation terms for the species CH_4, CH_2O and HCO. Note, that for a better comparability of the profiles the convection term has been inverted, so that at the leading edge of the flame all profiles of one diagram are positive or negative. Also, to provide better orientation the profiles of temperature have been added. Taking a look at the leading edge of the profiles one can see that for the 1143 K case the formation term of species in concordance with the heat release term in the energy equation increases prior to the diffusive sum term, while for 1083 K the opposite can be observed. This behavior is especially pronounced for the species CH_2O and CHO emphasizing the importance of these species for the auto-ignition process. As a result the temperature profile for the 1083 K case shows an unchanged (inlet) temperature up to the beginning of the peak of heat release and in the 1143 K case a significant temperature rise of at least 400 K prior to the main reaction zone can be seen.

As it is also interesting to take a look on the effect of diluted mixtures, additional calculations have been performed at varying equivalence ratio. Figure 10 shows selected results for two computational domain sizes and two equivalence ratios. It can be seen that the equivalence ratio has only negligible influence on the transition temperature while the influence of the domain size and the corresponding residence time upstream of the flame is larger.

3.5. Ignition delay time

The preceding discussion indicates that at preheating temperatures well above the auto-ignition temperature, the structure of the flame or reaction domain is similar to a reaction under plug flow conditions, i.e. without the contribution of diffusion or conduction. In order to validate the plug flow behavior of the reaction at high initial temperatures, the reaction progress has been quantified using the SENKIN program of the CHEMKIN II package [34],

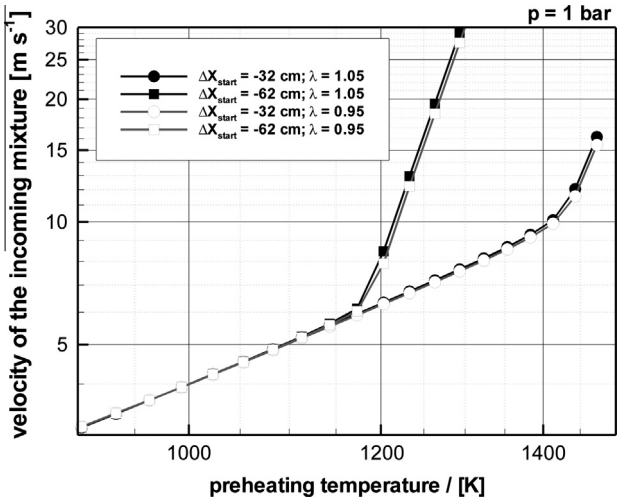

Fig. 10. Dependency of the incoming mixture velocity on preheating temperature varying equivalence ratio and domain size and using the GRI 3.0 mechanism at p_0 = 1 bar.

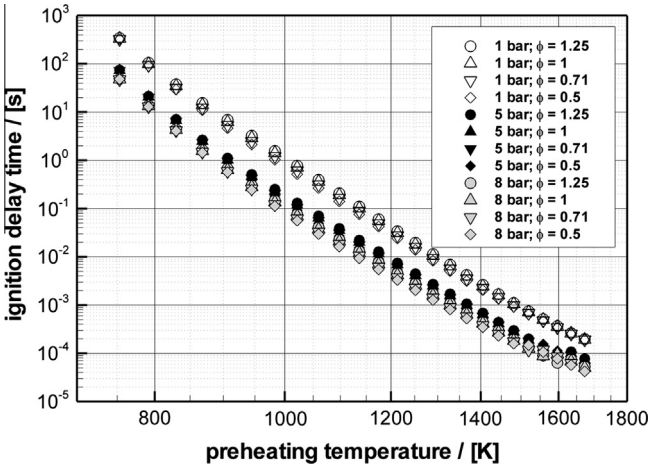

Fig. 11. Ignition delay times of methane–air mixtures as a function of the preheating temperature at different equivalence ratios and for three pressure levels p_0 = 1, 5 and 8 bar, calculated from the GRI 3.0 mechanism.

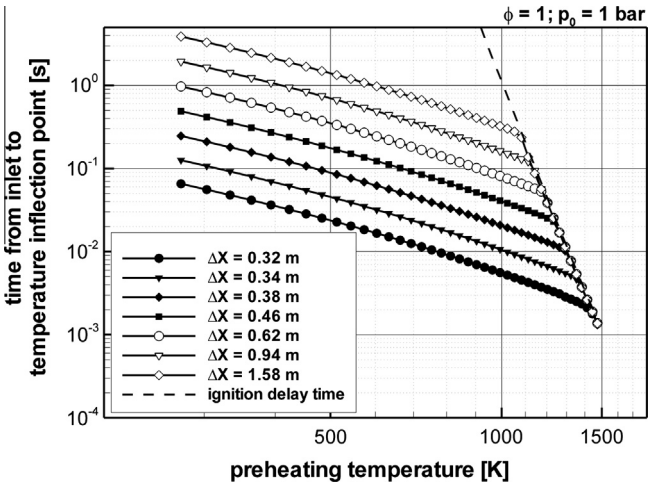

Fig. 12. Residence time from inlet to temperature inflection point (being characteristic for auto-ignition) as predicted from laminar, premixed flame calculations (lines with symbols) and ignition delay time (dashed line) predicted by the plug flow reactor model, as a function of unburned mixture preheating temperature (parameters: calculation domain size Δx in the laminar flame calculation, varied from 0.32 to 1.58 m; ϕ = 1.0, p_0 = 1 bar).

which calculates the species and temperature evolution in a transient homogeneous reactor. Assuming a constant mass flow in a plug flow reactor the position in such a reactor can be easily transformed to the time coordinate of the homogeneous reaction using the transformation rule $dt = \rho A \dot{M} dx$. Even though the used GRI 3.0 chemical-kinetic mechanism was not specifically optimized for the prediction of auto-ignition temperatures, it has been applied in the present work in order to provide comparability to the laminar flame calculations. Using the SENKIN program, ignition delay times have been calculated for methane–air mixtures at different initial pressures, temperatures and equivalence ratios (Fig. 11). The definition of the ignition delay time used in this work is the residence time of the reactants between the start of the calculation and the occurrence of an inflection point in the time evolution of the temperature in the homogeneous reactor. The consideration that auto ignition of the incoming mixture may be the reason for the steep increase of the laminar flame velocity in the high temperature region can be supported by comparing the residence time in the laminar flame calculation with the auto ignition time from the homogeneous reactor calculation.

For the laminar flame calculations a delay time can be defined using the time evolution of the concentration profiles and choosing the time duration that reactants travel in the laminar flame calculations from inlet to the temperature inflection point. This criterion has been used as well as other criteria commonly applied in literature for the determination of the ignition delay time like the time until a maximum of selected radical concentrations (e.g. C_2H_2) is reached. But, as the differences observed were small (5–10%) compared with the order of magnitude changes caused by a change of the preheating temperature, only the result of the temperature criteria is displayed. Figure 12 compares the so defined residence times for different sizes of the calculation domain (0.32–1.58 m), for stoichiometric methane/air mixture at 1 bar and for preheating temperatures from 900 to 1500 K. The extension of the calculation domain was done upstream of the flame, so that the residence time upstream of the flame increases accordingly.

In Fig. 12, these residence times are plotted together with the ignition delay times of Fig. 11 (dashed line). Figure 12 indicates that, for very high initial temperatures, the residence time up to the occurrence of the temperature inflection point from laminar flame calculations coincide with the curve of the ignition delay time of the homogeneous reactor calculation for all the studied different domain sizes. This result corroborates the evident idea that, if the incoming mixture is given sufficient time, the start of reaction is always controlled by auto-ignition provided the incoming mixture temperature is beyond a mixture-dependent threshold value called the "auto-ignition temperature". As a consequence of this control by ignition delay, diffusion plays only a very minor role for the initiation of combustion reactions, as to be seen from Fig. 12. As mentioned above the laminar burning velocity is independent of the domain length as long as the preheating temperature T_0 is below the auto-ignition temperature, as obvious from Fig. 8.

The behavior for high preheating temperatures (beyond auto-ignition) of the laminar flame is similar to that of the ideal plug flow reactor, where only the time delay is decisive for ignition, whereas the velocity may exhibit any arbitrary value. Different from a plug flow reactor computation, in the laminar premixed flame simulations, although the sum of diffusive terms does not control the start of the reaction, it still remains active in the energy equation and therefore the velocity that is required to balance the energy equation is determined by their dependence on gradients, i.e. derivatives with respect to the spatial coordinate, of temperature and species concentration. Consequently, when the reaction at high preheating temperature starts by auto-ignition, the velocity that is necessary to stabilize the stationary flame front is not only a characteristic of the mixture but also of the domain size. But, in contrast to the flame propagation domain the velocity is not an eigenvalue of the equations anymore but controlled by the ignition delay time. This is recognizable by the fact, that the flame location is not arbitrary anymore but controlled by the ignition delay time together with the flame velocity.

3.6. Effect of pressure

In order to explain the increase in the values of incoming mixture velocity with an increase in initial pressure, as shown in Fig. 2, for

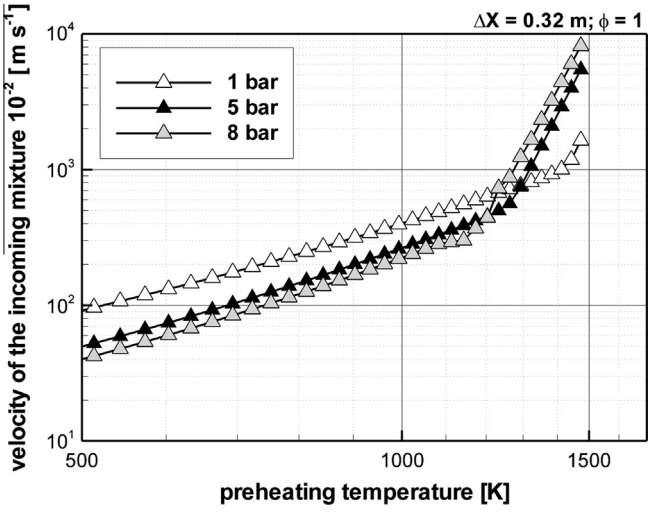

Fig. 13. Dependency of the incoming mixture velocity on preheating temperature for three different pressures (1, 5 and 8 bar) for methane/air mixture using the GRI 3.0 mechanism at $\phi = 1.0$.

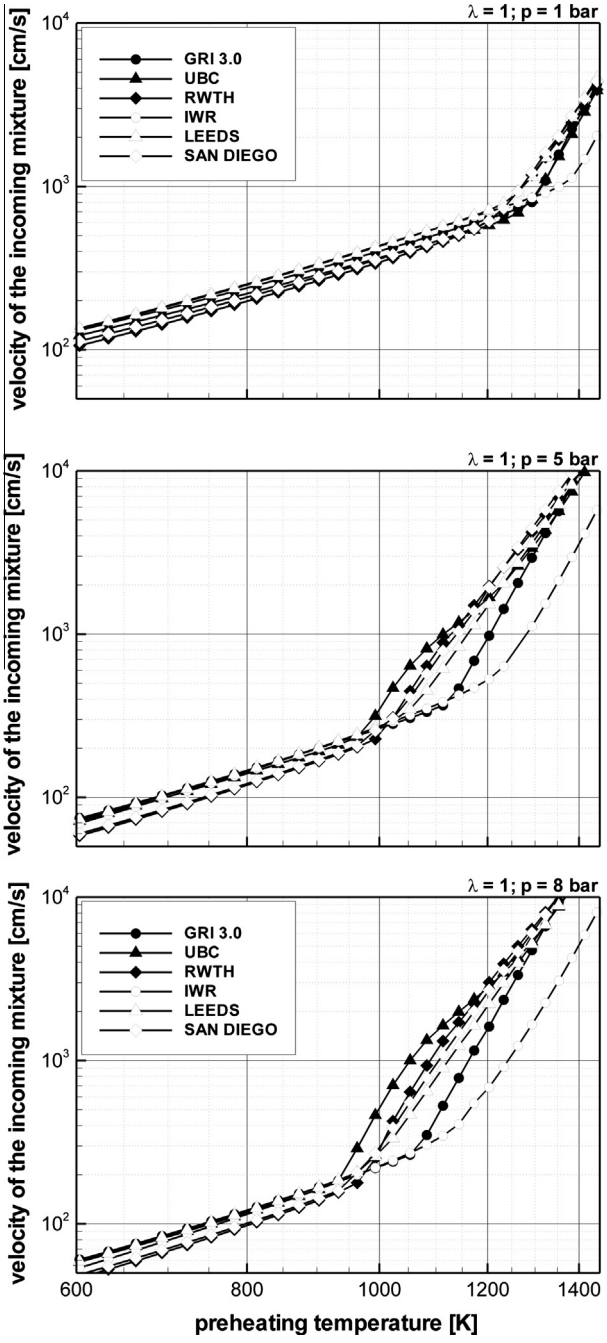

Fig. 14. Dependency of the incoming mixture velocity on preheating temperature using different chemical mechanisms, at $\phi = 1.0$ (top: $p_0 = 1$ bar; middle: 5 bar; bottom: 8 bar).

higher preheating temperatures, the comparison of the calculated incoming velocities of stoichiometric methane–air mixture as a function of the preheating temperature is shown in Fig. 13 for different pressures such as 1, 5 and 8 bar. The calculation domain is maintained constant at $\Delta x = 0.32$ m. Figure 13 ascertains the existence of two different regions, in which the burning velocity varies with change in pressure in the opposite direction. At preheating temperatures less than 1200 K (flame propagation domain), the laminar burning velocity always decreases with increase in pressure. In contrast to this and analogous to Fig. 2, the incoming velocity increases with increasing pressure for preheating temperatures above the range between 1200 K and 1450 K (auto-ignition domain). Moreover, the transition of the two domains of flame behavior shifts to lower preheating temperatures with increasing pressure and occurs in a narrow temperature range. It is essential to mention, that as a consequence of the considerations above, for the given example in the preheating temperature range from 1250 K to 1400 K the pressure level is the decisive quantity for the type of flame stabilization mechanism: while at 1300 K and 1 bar the flame front is controlled by flame propagation the behavior changes to control by auto-ignition at 1300 K and 5 bar or 8 bar.

In order to cross-validate the observed result for calculations with the GRI 3.0 mechanism the calculations have been repeated using the UBC, RWTH, IWR, LEEDS and SAN DIEGO mechanisms. Figure 14 shows that for all of the applied chemical schemes results with a simular trend can be obtained while the transition temperature varies between 1200 K (RWTH) and 1400 K (IWR) at 1 bar, between 950 K (UBC) and 1200 K (IWR) at 5 bar and between 900 K (UBC) and 1100 K (IWR) at 8 bar. The RWTH, LEEDS and SAN DIEGO mechanisms show very similar trends while the UBC and IWR mechanisms for all applied pressure levels show the lowest respectively the highest transition point. The velocities resulting from using the GRI 3.0 mechanism is in all cases are in between the extremes. The observed dependency of the laminar flame speed (low temperature range) of the mechanisms agree well within a range of 5%.

To understand the change in the effect of pressure on the burning velocity at higher initial temperatures, the energy equation terms are plotted in Fig. 15 for two initial temperatures, $T_0 = 600$ K in the top row and $T_0 = 1450$ K in the bottom row for different pressures such as 1, 5 and 8 bar. Figure 15 shows that at $T_0 = 600$ K and 1 bar, the reaction zone in the flame spans the shortest time, and the absolute value of the diffusive sum term in the energy equation increased prior to the energy release term. The same trend is to be observed for other pressures such as 5 and 8 bar. Figure 15 indicates that at $T_0 = 1450$ K, however, the profile

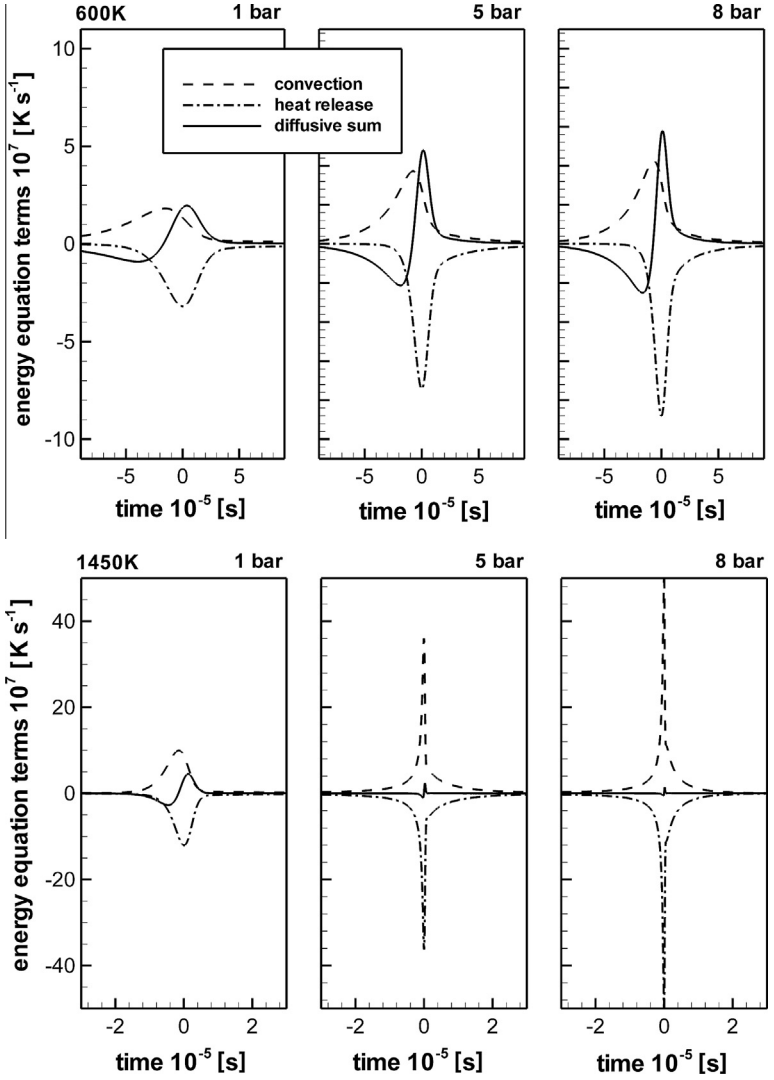

Fig. 15. Profiles of the terms of the energy equation for CH_4/air mixture, $\phi = 1.0$, with pressures of 1, 5 and 8 bar using the GRI 3.0 mechanism. Unburned mixture temperature T_0 is 600 K (top) and 1450 K (bottom).

of the diffusive sum term in the flame undergoes a drastic change with an increase in the pressure from 1 to 5 bar. At 1 bar and 1450 K, the diffusive sum terms begins to raise slightly before the raise in the energy release term, while at 5 and 8 bar the onset of increase in the absolute value of the energy release term profile clearly precedes the diffusive sum term. This indicates again that the chemical reaction at 1450 K and pressures at 5 and 8 bar is approaching a condition similar to that of a plug flow reactor, i.e. in the auto-ignition domain.

3.7. Limit of flame propagation mode

At low initial temperatures, the laminar burning velocity is the velocity of the incoming fluid. If one assumes, following Zeldovic and Frank-Kamenetsky, that the density and, thus, the velocity upstream of the inflection point would be approximately constant, then, the residence time of the reactants from the inlet (or "flame foot") position to the temperature inflection point (tp) can be approximated as $\tau_{tp} = \Delta x_{tp}/S_L$. At these conditions, the flame is stabilized by means of flame propagation, i.e. a portion of the energy released in the reaction zone is being transported by diffusive processes back to the preheat zone for preheating the reactants above the self-ignition temperature in order to achieve a sustainable flame.

At the transition point of preheating temperature, where the flame behavior changes from self propagation to ignition delay control, the residence time of the reactants equals the ignition delay time τ_{id} for auto-ignition at inlet temperature, and hence the distance between the inlet and the position of the occurrence of the inflection in the temperature profile Δx_{tp} may be simply approximated as:

$$\Delta x_{tp} = \tau_{id} \cdot S_L \tag{7}$$

since mixture density between inlet (or beginning of calculation domain) and auto-ignition point is really constant. The ignition delay time mentioned in the above equation, as well as the laminar flame speed S_L is a function of inlet temperature, pressure and equivalence ratio. There is a wide range of ignition delay time that spans six orders of magnitude for a range of inlet temperature from 800 to 1600 K (Fig. 8). For this reason, if the computational domain chosen for the simulations of a combustible mixture well above its auto-ignition temperature is small enough such that the residence time of the reactants is shorter than the auto-ignition delay time of the corresponding mixture, then a laminar flame will stabilize by means of diffusive controlled flame propagation under such conditions. Of course, flames burning under those conditions certainly exhibit quite high laminar burning velocities. And, in addition, if the computation domain upstream of the flame is then increased above the limit expressed in Eq. (7), the position of the reaction zone will change over to depend on the residence time of the reactants, i.e. to immediate auto-ignition at the mixture inlet. Therefore, for the above mentioned conditions, the flame is stabilized by means of auto-ignition, no more by flame propagation which would occur, independent of the size of the computational domain.

4. Conclusions

The analysis of the results of freely propagating, one dimensional, laminar premixed flames of stoichiometric methane–air mixture for different inlet temperatures ranging from 298 K to 1450 K and at different pressures from 1 to 8 bar indicates that:

For inlet temperatures less than 1000 K and at 1 bar, the laminar burning velocity decreases with increased pressures, and this trend of variation agrees well with experimental data and the thermal theory of laminar flame propagation.

If the inlet temperature increases well above the limit of auto-ignition temperature, then the velocity of the incoming mixture increases with increased pressures. The present analysis of different energy terms in the energy equation shows that this behavior is due to a change in the flame structure induced by the ignition delay time for auto-ignition, which is a strong function of the inlet temperature.

For inlet temperatures below the auto-ignition temperature, the flame structure comprises a thick preheating zone and a comparatively thin reaction zone, and the flame is stabilized by means of diffusive controlled flame propagation. For inlet temperatures well above the auto-ignition temperature of the studied mixture, the relative influence of the diffusive sum terms in the energy balance equation decreases drastically due to an increase of the heat release term which results in very high burning velocities. A limiting criteria based on the ignition delay time has been formulated in order to distinguish with regard to the stabilization mechanism of a flame between laminar flame propagation and auto-ignition.

An essential result is also the pressure dependency of the flame front behavior at high preheating temperatures. As a consequence for a secondary stage combustion system, when the stabilizing mechanism is due to flame propagation for low pressure levels, with an increase of pressure the stabilization region of the secondary stage injection will move downstream of the fuel injection point due to a decrease of the laminar and therefore also of the turbulent flame speed. However, in the case of stabilization due to the auto-ignition at higher preheating temperature an increase of pressure will reduce the ignition delay time and therefore the stabilization region will move upstream to the injection point. Because of the strong dependency of the ignition delay time on pressure the pressure dependency of the stabilization region can even change by increasing pressure as described above.

References

[1] T. Hasegawa, S. Mochida, A.K. Gupta, AIAA J. Propul. Power 2 (2002) 233–239.
[2] J.A. Wünning, J.G. Wünning, Prog. Energy Combust. Sci. 23 (1997) 81–94.
[3] A. Cavaliere, M. de Joannon, Prog. Energy Combust. Sci. 30 (2004) 329–366.
[4] T. Weydahl, M. Poyyapakkam, M. Seljeskog, N. Erl, L. Haugen, Int. J. Hydrogen Energy 36 (2011) 12025–12034.
[5] S. Hayashi, H. Yamada, Proc. Combust. Inst. 28 (2000) 2443–2449.
[6] C. Prathap, F.C.C. Galeazzo, P. Kasabov, P. Habisreuther, N. Zarzalis, C. Beck, W. Krebs, B. Wegner, J. Eng. Gas Turb. Power 134 (3) 031507-031507-8, http://dx.doi.org/10.1115/1.4004720.
[7] Y. Ogami, H. Kobayashi, JSME Int. J., Ser. B 48 (3) (2005) 603–609.
[8] S.P. Sharma, D.G. Agrawal, C.P. Gupta, Proc. Combust Inst. 18 (1981) 493–501.
[9] M.G. Zabetakis, Bureau Min. Bull. 627 (1965) 1–121.
[10] K.C. Smyth, N.P. Bryner, Combust. Sci. Technol. 126 (1997) 225–253.
[11] M. Caron, M. Goethals, G. De Smedt, J. Berghmans, S. Vliegen, E. Van't Oost, A. van den Aarssen, J. Hazard. Mater. 65 (1999) 233–244.
[12] D.J. Seery, C.T. Bowman, Combust. Flame 14 (1970) 37–47.
[13] A. Lifshitz, K. Scheller, A. Burcat, G.B. Skinner, Combust. Flame 16 (1971) 311–321.
[14] T. Tsuboi, H.G. Wagner, Proc. Combust. Inst. 15 (1974) 883.
[15] R.K. Cheng, A.K. Oppenheim, Combust. Flame 58 (1984) 125–139.
[16] A. Grillo, M.W. Slack, Combust. Flame 27 (1976) 377–381.
[17] J. Huang, P.G. Hill, W.K. Bushe, S.R. Munshi, Combust. Flame 136 (2004) 25–42.
[18] G. Rozenchan, D.L. Zhu, C.K. Law, S.D. Tse, Proc. Combust. Inst. 29 (2002) 1461–1469.
[19] M.I. Hassan, K.T. Aung, G.M. Faeth, Combust. Flame 115 (1998) 539–550.
[20] F.N. Egolfopoulos, P. Cho, C.K. Law, Combust. Flame 76 (1989) 375–391.
[21] E. Hu, Z. Huang, J. He, H. Miao, Int. J. Hydrogen Energy 34 (16) (2009) 6951–6960.
[22] R.J. Kee, J.F. Grcar, M.D. Smooke, J.A. Miller, A Fortran Program for Modeling Steady Laminar One-Dimensional Premixed Flames, Sandia Report SAND89-8009, Sandia National Laboratories, 1993.
[23] R.J. Kee, F.M. Rupley, J.A. Miller, A Fortran Chemical Kinetics Package for the Analysis of Gas Phase Chemical Kinetics, Sandia Report SAND85-8240, Sandia National Laboratories, 1991.
[24] G.P. Smith, D.M. Golden, M. Frenklach, N.W. Moriarty, B. Eiteneer, M. Goldenberg, C.T. Bowman, R.K. Hanson, S. Song, W.C. Gardiner Jr., V.V. Lissianski, Z. Qin, GRI-Mech Homepage <http://www.me.berkeley.edu/gri_mech/>.

[25] C.T. Bowman, R.K. Hanson, D.F. Davidson, W.C. Gardiner Jr., V. Lissianski, G.P. Smith, D.M. Golden, M. Frenklach, M. Goldenberg, GRI-Mech Homepage <http://www.me.berkeley.edu/gri_mech/>.
[26] K.J. Hughes, T. Turànyi, A.R. Clague, M.J. Pilling, Int. J. Chem. Kinet. 33 (9) (2001) 513–538.
[27] Chemical-Kinetic Mechanisms for Combustion Applications, San Diego Mechanism web page, Mechanical and Aerospace Engineering (Combustion Research), University of California at San Diego <http://combustion.ucsd.edu>.
[28] S. Honneta, K. Seshadrib, U. Niemannb, N. Peters, Proc. Combust. Inst. 32 (2009) 485–492.
[29] Y. Muharam, J. Warnatz, Phys. Chem. Chem. Phys. 31 (9) (2007) 4218–4229.
[30] J. Huang, P.G. Hill, W.K. Bushe, S.R. Munshi, Int. J. Chem. Kinet. 38 (4) (2006) 221–233.
[31] Ya.B. Zeldovich, D.A. Frank-Kamenetsky, Zh. Fiz. Khim. 12 (1) (1938) 100–105.
[32] M.W. Evans, Chem. Rev. 51 (1952) 363–429.
[33] O.C. Kwon, G.M. Faeth, Combust. Flame 124 (2001) 590–610.
[34] A.E. Lutz, R.J. Kee, J.A. Miller, A FORTRAN Program for Predicting Homogeneous Gas Phase Chemical Kinetics with Sensitivity Analysis, Sandia Report SAND87-8248, Sandia National Laboratories, 1988.